

Damage analysis of glass fiber reinforced composites

7

Syafiqah Nur Azrie Bt Safri¹, M.T.H. Sultan^{1,2,3}, Mohammad Jawaid²

¹Aerospace Manufacturing Research Centre (AMRC), Faculty of Engineering, Universiti Putra Malaysia, Serdang, Malaysia; ²Laboratory of Biocomposite Technology (BIOCOMPOSITE), Institute of Tropical Forestry and Forest Products (INTROP), Universiti Putra Malaysia, Serdang, Malaysia; ³Department of Aerospace Engineering, Universiti Putra Malaysia, Serdang, Malaysia

7.1 Introduction

Composite materials are important in structural industry, the aerospace industry, and the automotive industry as these require lightweight and strong materials. Composite materials have been manufactured as early as 3000 BC, when natural fiber and stone composites were used for housing in the Middle East during the time of Sumerians [1]. Nowadays, one of the best known fibers used to make composites is fiberglass. Glass fibers were made from molten mixture of dolomite, limestone, quartz sand and paraffin, with a little combination of boric acid and soda [2]. In 1939, glass fiber was used in US navy warships as insulator. Glass fiber was also used for structural parts of aircraft during World War II. Glass fiber is a more common choice for industries compared to Kevlar and carbon fiber because it is economically cheaper. Fig. 7.1 shows the best properties of glass fiber.

Glass fiber is low in density and Young's modulus, but it has high strength. It is also durable in various environmental conditions. Glass fiber is also one of the common materials tested by researchers by combining it with various matrices and reinforcements. Table 7.1 shows previous research for glass fiber hybrid composites.

This chapter presents an experimental investigation using high velocity impact testing to detect and quantify the impact damage sustained by Glass Fiber Reinforced Polymer (GFRP) type E-800 g/m² and type C-600 g/m² panels. GFRP type E-800 g/m² and type C-600 g/m² plates were tested using a single stage gas gun (SSGG). This research investigated the effect of specimen thickness, the type of projectiles and the impact velocity on the failure modes of GFRP type E-800 g/m² and type C-600 g/m² using non-destructive testing methods.

7.2 Impact testing

There are two different impact tests that are typically used for composite materials, which are low velocity impact testing and high velocity impact testing. Fig. 7.2 shows the damage experienced by the composites during low velocity impact testing.

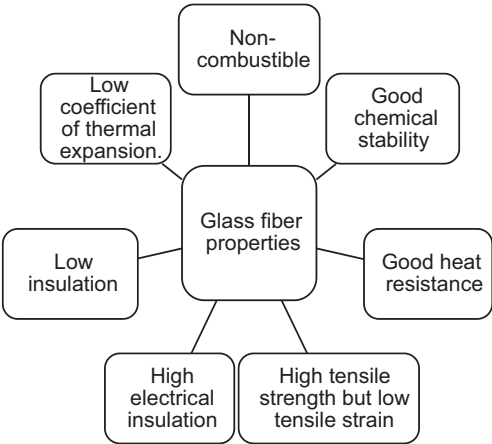


Figure 7.1 Glass fiber properties.

Table 7.1 Reported research on glass fiber reinforced hybrid composites

Hybrid	Year	References
Glass–cotton fiber	2012	[3]
Glass–hemp fiber	2015	[4]
Glass–Kevlar–carbon fiber	2017, 2016, 2015, 2014	[5–8]
Glass–hemp–basalt–flax fiber	2015	[9]
Glass–kenaf fiber	2016, 2015, 2014	[10–12]
Glass–basalt fiber	2010	[13]
Glass–Kevlar fiber	2017, 2015	[14,15]
Glass–jute fiber	2016, 2015	[16,17]
Glass–carbon fiber	2016, 2015, 2013	[18–23]
Glass–flax fiber	2017, 2016	[24,25]
Glass– <i>P. purpureum</i> grass fiber	2016	[26]
Glass–sisal fiber	2017, 2011	[27,28]
Glass–curaua fiber	2017	[29]
Glass–tamarind fiber	2015	[30]
Glass–bamboo fiber	2014	[31]
Glass–sisal–jute fiber	2016	[32]

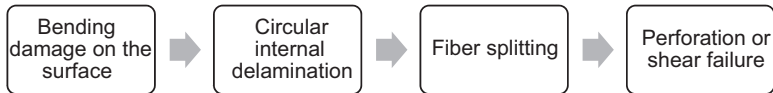


Figure 7.2 Damage modes for low velocity impact testing.

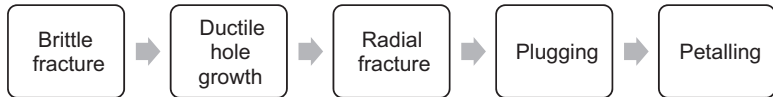


Figure 7.3 Failure modes for high velocity impact testing.

However, for high velocity impact testing, there are different types of damage experienced by the composites because the impact provides higher frequency mode thus inducing the deformation field. Fig. 7.3 shows the failure mode for high velocity impact testing.

When a composite experiences impact, the composite strength and stiffness are reduced since the internal damage is made and expanded around the impact area. The projectile kinetic energy was changed into plastic deformation before perforation occurred. This happened because of better bending stiffness of the impacted plate. Potential damage modes in composites that have been subjected to impact loading are matrix cracking, interfacial debonding, lamina splitting, delamination, fiber breakage, and fiber pullout.

7.2.1 Matrix cracking

The first type of failure is matrix cracking. It usually happens because of a low velocity impact event, followed by matrix tension, compression, and shearing. Examples of matrix cracking are shear cracking (inclination of 45°) and bending cracking (vertical inclination). After impact events, matrix cracking is the first damage on the impacted composites that cannot be seen with the naked eye. Matrix cracking will reduce the compression strength and interlaminar shear of the composite interface.

7.2.2 Delamination

Delamination is the most crucial damage for impacted composite. Delamination occurs from the layers in the composite laminate. Delamination is caused by matrix cracking, bending cracks, and shear cracks. Delamination can affect the compression strength of composite laminate, and it will slowly cause the composite to experience failure through buckling. Stress experienced by the composite initiates cracks and causes delamination between the laminates and leads to more severe damage. During low or high velocity impact event, when a composite laminate experiences impact, several damage modes can occur, including matrix crack, delamination, fiber crack, and fiber pullout. All of these damage modes are dependent on the impact parameter such as impact energy and impactor mass or impactor shape [33]. A Bigger impactor will

result in greater delamination if there no penetration occurs. If there is any penetration experienced by the composite, the delamination is less because the material did not deflect as much as it could. A Blunt impactor will also result in more delamination compared to other shapes of impactor [34].

7.2.3 Fiber failure

Fiber pullout and fiber breakage are the most common failures under low velocity impact testing. Fiber failure occurs because of the high stress field and indentation effects. The projectile induces a shear force and high bending stresses in the nonimpacted side of the specimen. Fiber breakage is one of the steps towards the final failure of composites. In fiber bundle theory, the final tensile failure of the composite occurs when a certain number of fiber breakages occur. Fiber breakage can occur as a result of high stresses or a sudden rise in temperature during the experimental work or as an indentation effect. Fiber breakage can damage the mechanical performance of composite materials [35]. During impact tests, the impactor shape affects the fiber breakage; for example, when the specimens are impacted by the hemispherical impactor, there is more delamination in the specimens, whereas specimens impacted by an ogival impactor have more fiber breakage [34]. The impacted specimens experienced highly localized fiber breakage as there is a formation of a plug below the impactor [36]. The type of fiber affects the severity of the fiber breakage; for example, the fiber magnitude of stress and strain during fiber processing and the fiber initial aspect ratio.

7.3 Damage analysis using Non-destructive Evaluation (NDE)

Impact damage sometimes cannot be seen easily using the human eye. This type of damage is called barely visible impact damage (BVID). There are several techniques that can be used to analyze the damage on composite structures. One of the most famous techniques is using non-destructive evaluation (NDE). NDE is often used in the aircraft industry, structural applications, and other related industries. This technique helps to detect damage thus avoiding any possible accident that may occur. The detection of the damage is the first step in technical diagnosis, and it can be used to determine the extent of the damage. NDE will detect different damage types, such as voids and delaminations. One of the most commonly used techniques for composites is ultrasonic testing (UT), usually using the C-scan transmission or A-scan transmission. UT can detect porosity, delaminations, and internal voids. Ultrasonic methods are capable of scanning images with greater speed because the ultrasonic passed array can focus the beam while inspecting the composites. UT for defect detection is carried out using ultrasonic waves at high frequencies above the audible range, higher than approximately 20 kHz and up to the range of several hundred MHz. One of the traditional and economical methods of NDE is visual inspection. This is a technique where the composite surface is evaluated solely using the human eye. In the aircraft industry, visual inspections are important for damage assessment and quality

control. Usually, the technicians are using other tools as aids, including flashlights, mirrors, and magnifying glasses. Normally, composite surface roughness, porosity, ply distortions, and wrinkles can be assessed using this method.

7.4 Experimental procedure for damage detection

The composite materials chosen are woven-roving GFRP type C-600 g/m² and type E-800 g/m². These woven roving materials were laminated with epoxy resin to increase their impact strength. The materials were fabricated using a hand lay-up technique with the aid of a hot-press machine. The process of preparing the compound was based on a 2:1 ratio, that is, two portions of epoxy to one portion of hardener by mass. The epoxy resin and hardener used were from types Zeepoxy HL002 TA and Zeepoxy HL002 TB. For the high velocity impact tests, GFRP type E-800 g/m² and type C-600 g/m² were fabricated into four different thicknesses, 6 mm, 8 mm, 10 mm, and 12 mm. Specimen plates with a size of 100 mm × 100 mm for both types of glass fiber were cut using a CNC router machine. High energy impact tests were carried out using an SSGG at the Faculty of Manufacturing Engineering, Universiti Malaysia Pahang. In this test, specimens with dimensions of 100 mm × 100 mm were impacted with three types of projectiles: blunt, conical, hemispherical. The speeds of the projectiles are varied using the gas gun. In this test, the projectile velocity range is within 70–240 m/s.

For low velocity impact tests, 120 specimen plates as per the Boeing Specification Support Standard BSS 7260 (100 mm × 150 mm) for both types were cut using a CNC router machine. The thickness for each material is shown in Table 7.2.

Table 7.2 compares the average thicknesses of the laminates. The thicknesses were measured after the curing process. The standard deviation were the same because the thickness of the fabricated specimens is almost the same. This is because the same procedure has been used to fabricate all the specimen. It shows that glass fiber type E-800 g/m² produced much thicker laminates compared with type C-600 g/m² for

Table 7.2 Laminate thickness for type C-600 g/m² and type E-800 g/m²

Type of fiber glass	Number of plies	Average thickness, (mm)
C-600 g/m ²	10	6.0 ± 0.10
	12	7.0 ± 0.12
	14	8.0 ± 0.09
E-800 g/m ²	10	7.0 ± 0.11
	12	8.0 ± 0.10
	14	9.0 ± 0.12

the same number of plies. Tests were performed using a drop weight testing machine on different sample thicknesses to achieve different impact responses.

The striker was 0.787 kg in weight and had a hemispherical geometry shape, with a tip radius of 5 mm. The total drop mass was 8.891 kg. Two types of glass fiber, type E-800 g/m² and type C-600 g/m² with three thicknesses of laminate, 10, 12, and 14 plies, were considered. For the 12-ply and 14-ply specimens, for both types of glass fiber, a total of 96 plates were used in the impact tests at eight different energy levels. The impact energies for the 12-ply and 14-ply specimens were 6, 12, 18, 24, 30, 36, 42, and 48 J. However, for 10-ply specimens, for both types of glass fiber, a total of 24 plates were used to perform the impact test at four energy levels, 12, 24, 36, and 48 J due to material and cost limitations. For each type of energy, three samples were subjected to impact in order to obtain data repeatability. The reason for performing the repeatability test was to check the accuracy of the measurements.

7.4.1 Dye penetrant

The impact damage on the specimen was examined using the dye penetrant technique and an optical microscope. Dye penetrant testing follows the basic rules of capillary action where the penetrant enters the damage composite and reemerges on the surface after applying the developer. The dye penetrant used is Spotcheck SKL-SP2, which is a solvent-removable (or postemulsifiable) red color contrast penetrant with outstanding penetrating characteristics. Spotcheck SKL-SP2 is accommodating with ASME B & PV Code Sec V and the ASTM E1417 standard.

7.4.2 Optical microscope

An optical microscopy examination of the sectioned specimens was performed to detect the main damage modes over the impact zones. Delamination, matrix cracking, matrix breakage, fiber cracking, and fiber breakage were observed from the microstructure of the damaged specimens. The optical microscope used, the Olympus BX51 microscope, is available in the Aerospace Composite Laboratory, Faculty of Engineering, Universiti Putra Malaysia. The capabilities of the BX51 include Nomarski differential interference contrast (DIC), fluorescence, dark-field, and polarization microscopy. The advantages of using this optical microscope (Olympus BX51) are as follows: its superb optical performance, outstanding fluorescence capability, and optimized contrast and resolution. The optical microscope is capable of great magnification. However, the level of magnification chosen in this test is 5 times. The optical microscope is interfaced to a computer software called analySIS. It is a software for image acquisition, archiving, processing, and analysis. The results obtained from high velocity impact and low velocity impact testing of glass fiber type E-800 g/m² and type C-600 g/m² are thoroughly discussed and presented. The analysis of the types of damage suffered from the impact tests using dye penetrant and an optical microscope is presented. The failure mode experienced by the specimens is analyzed.

7.5 Results from the dye penetrant testing

Fig. 7.4 shows the average damaged area in m^2 for the panels with 6 mm, 8 mm, 10 mm, and 12 mm of thickness. From (a) to (d), it is shown that as the gas gun pressure increases, the damaged area also increases. This is because, as the gas gun pressure increases, the impact force also increases resulting in a corresponding larger damage area. By comparing both types of glass fiber, most of the tests show that glass fiber type E-800 g/m^2 has smaller damage than type C-600 g/m^2 . This result was due to the fact that type E-800 g/m^2 is stronger due to its higher fiber strength, in comparison with the type C-glass fiber, as previously discussed. However, there were certain tests where the damage area of type C-600 g/m^2 was much more smaller than for the type E-800 g/m^2 . This may have occurred as a result of the fabrication process, where the

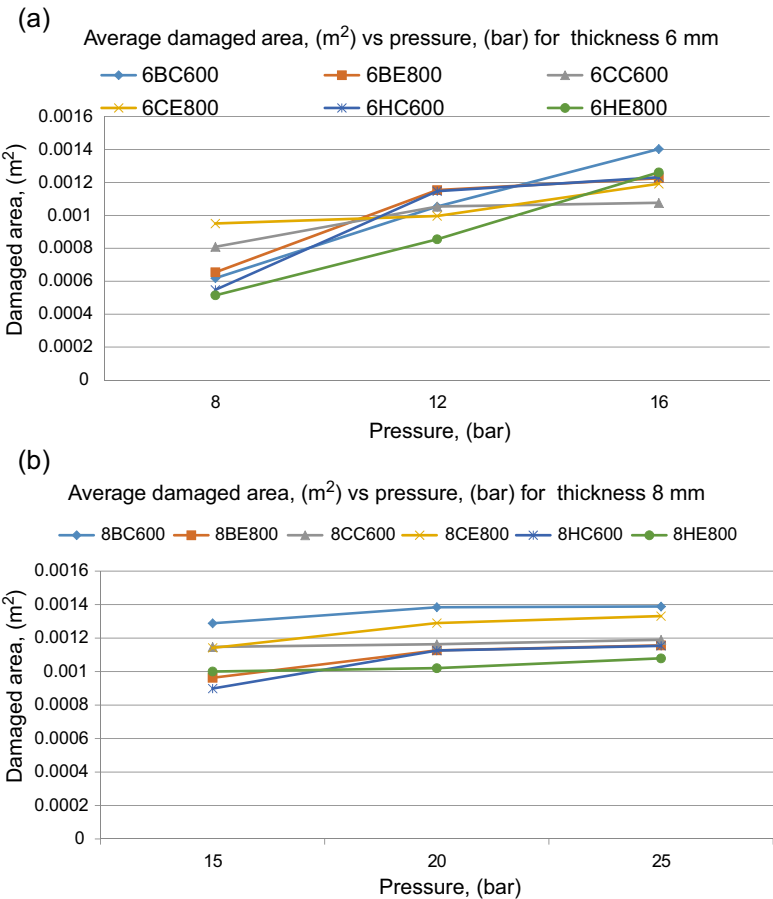


Figure 7.4 Average damaged area versus pressure for the panels with type E-800 g/m^2 and type C-600 g/m^2 for (a) 6 mm (b) 8 mm (c) 10 mm (d) 12 mm.

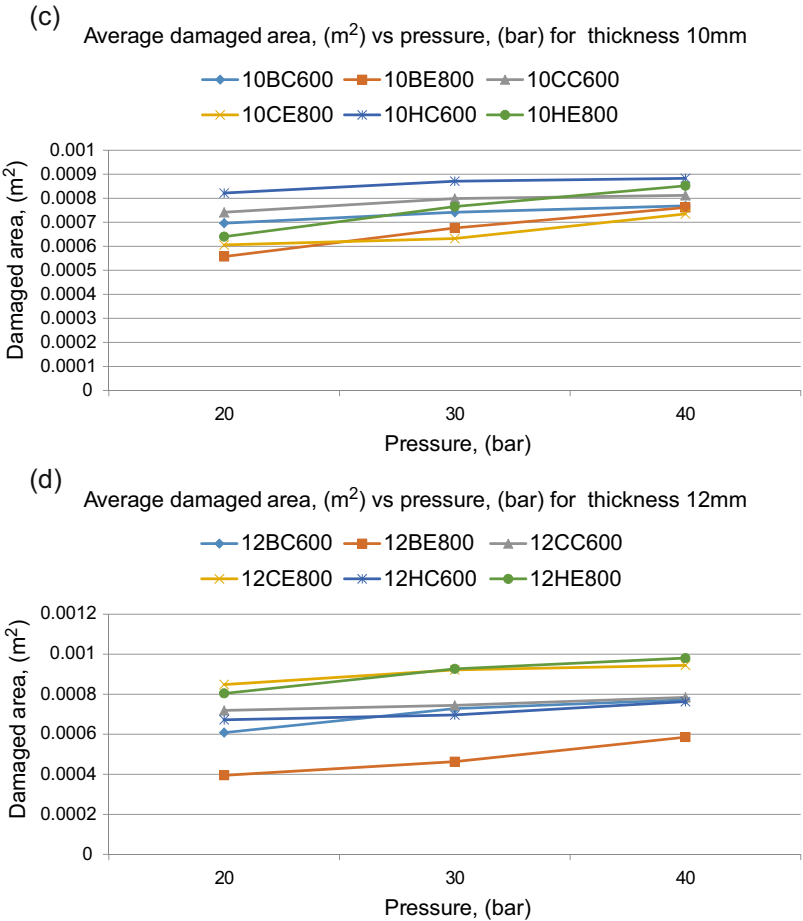


Figure 7.4 cont'd.

percentage content of the resin in the laminate was comparatively high. If there is too much resin in the laminate in relation to the content of fiber reinforcement, the whole laminate becomes brittle. In relation to the shape of the projectiles, the results, however, are not consistent. This maybe due to the fact that the initial velocity of each projectile was different because its mass was also different. It was found from these figures that as the thickness of the target plate increased, more resistance was offered by the target plates to perforation by the projectile. A linear relationship was found between the impact velocity and the damage area. The higher the impact velocity, the greater the damaged area. Therefore, it was found that type E-800 g/m² is stronger than type C-600 g/m².

Fig. 7.5 shows the average damaged area in m² for glass fiber type C-600 g/m² and type E-800 g/m². As the impact energy increases, the damage area also increases for all

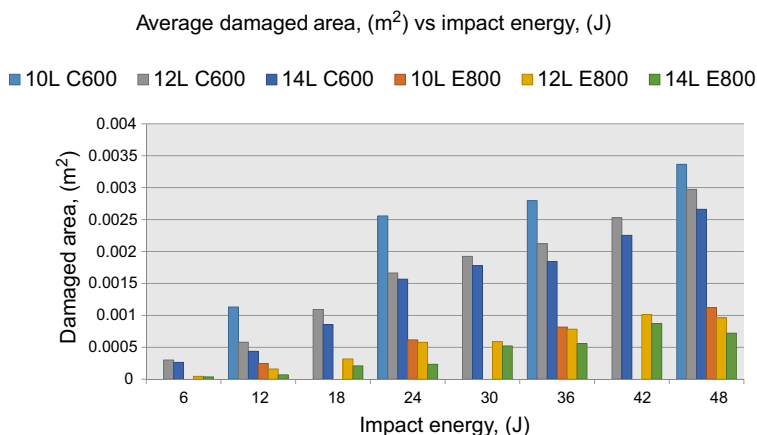


Figure 7.5 Damaged area versus impact energy for type C-600 g/m² and type E-800 g/m². It is the average value of each set of samples at each impact energy. The damaged area experienced by the specimen was measured after the impact test.

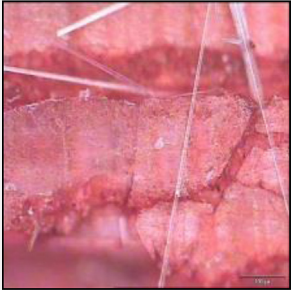

tested specimens. However, as the specimen thickness increases, the specimen damage area decreases due to the increase ability to absorb the impact energy [37]. According to Sevkati et al. [38], when the energy absorbed by the composite is small, the impactor bounced back and the damage area is also small. Glass fiber type E-800 g/m² experienced less damaged area for all thicknesses compared with glass fiber type C-600 g/m². This is because glass fiber type E-800 g/m² is higher in strength compared to glass fiber type C-600 g/m².

7.6 Optical microscope analysis

Optical inspection was performed on the impacted specimens to identify the failure mode. The damage modes were fiber breakage accompanied by matrix cracks, delaminations, penetrations, and perforations. Before this deformations occurred, the specimens would first experienced matrix cracking and delamination. For the high velocity impact test, multiple cracks occurred on the back surface of the specimens and fibers break under impact point. Outside the ply failure zone, delaminations extended from the tips of the matrix (cone) cracks [39].

Table 7.3 shows an example of failure mode that happened to one of the impacted specimens. Some of the impact energy was transferred to the laminate in the form of kinetic energy, if the impact velocity was equal to or lower than the ballistic limit, and then the laminate displacement resulted in fiber failure and elastic deformation of the laminate. At the end of the impact event, the kinetic energy was reduced to zero, and all the energy previously transferred to the laminate is absorbed by other mechanisms [40]. Both glass fiber types showed damage in terms of fiber cracking

Table 7.3 Example of failure mode suffered by the impacted specimen

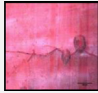
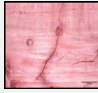
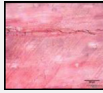
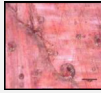
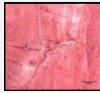
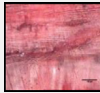
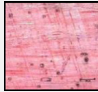
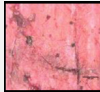


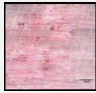
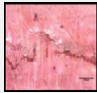
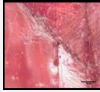

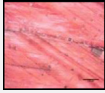
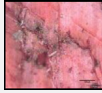
Fiber crack	Fiber pullout
	

and fiber pullout after being tested with four different gas gun pressures. Before fiber failure occurs, the laminates will first undergo matrix cracking and delamination processes.

Table 7.4 shows the failure mode at the impacted surface area for 10-ply, 12-ply, and 14-ply glass fiber type C-600 g/m² and type E-800 g/m². The 10-ply type C-600 g/m² specimens exhibited more severe matrix damage than the other tested specimens. 14-ply type E-800 g/m² experienced less impact damage because it is thicker than the other tested specimens. At the energy level of 12 J, for 14-ply type E-800 g/m², delamination occurs. However, for 14-ply type C-600 g/m², the failure mode was matrix crack. Type C-600 g/m² specimens exhibited more severe matrix damage than the type E-800 g/m² at the same impact energy level. This shows that glass fiber type E-800 g/m² is stronger than glass fiber type C-600 g/m².

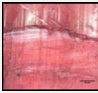

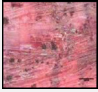
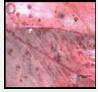
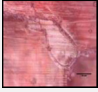
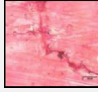

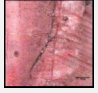
At impact energy 48 J, for 10-ply type E-800 g/m², the failure mode was only fiber cracking. On the other hand, for 10-ply type C-600 g/m², the failure mode was fiber breaking. 14-ply type E-800 g/m² only experienced matrix cracking and 14-ply type C-600 g/m² also exhibited matrix cracking when impacted at the highest impact energy, 48 J. This shows that as the number of plies increased, the failure becomes more lenient. At impact energies lower than 12 J, the damages were less severe compared with the specimens under a 48 J impact load. In this experiment, several damage modes have been detected. At impact energies lower than 12 J impact load, the main damage modes were delamination and matrix crack rather than fiber crack or fiber break. For higher impact energies of 48 J, fiber crack and fiber break were noticed around the site of impact. These fragmentation results were expected; the damage areas increased as the impact energy increased. For both types of glass fiber, for specimens that are damaged by 12–48 J impact energy, matrix cracks were observed on the damaged surface and delaminations in the cross-section and on the inner surface of the specimens, except for 14-ply type E-800 g/m² and 12-ply type E-800 g/m² at impact energy 12 J.

Table 7.4 Microscopic images for type C-600 g/m² and type E-800 g/m²

		Impact energy, 12 J	Impact energy, 24 J
10-ply type C-600 g/m ²	Specimen		
	Failure mode	Matrix crack	Matrix break
10-ply type E-800 g/m ²	Specimen		
	Failure mode	Matrix crack	Matrix break
12-ply type C-600 g/m ²	Specimen		
	Failure mode	Matrix crack	Matrix break
12-ply type E-800 g/m ²	Specimen		
	Failure mode	Delamination	Matrix crack
14-ply type C-600 g/m ²	Specimen		
	Failure mode	Matrix crack	Matrix crack
14-ply type E-800 g/m ²	Specimen		
	Failure mode	Delamination	Matrix crack
		Impact Energy, 36 J	Impact Energy, 48 J
10-ply type C-600 g/m ²	Specimen		
	Failure mode	Fiber crack	Fiber break
10-ply type E-800 g/m ²	Specimen		
	Failure mode	Fiber crack	Fiber crack

Continued

Table 7.4 Continued

		Impact Energy, 36 J	Impact Energy, 48 J
12-ply type C-600 g/m ²	Specimen		
	Failure mode	Fiber crack	Fiber crack
12-ply type E-800 g/m ²	Specimen		
	Failure mode	Matrix crack	Fiber crack
14-ply type C-600 g/m ²	Specimen		
	Failure mode	Matrix crack	Matrix crack
14-ply type E-800 g/m ²	Specimen		
	Failure mode	Matrix crack	Matrix crack

7.7 Conclusion

In the work carried out and presented here, the failure mode of the glass fiber impacted specimens have been thoughtfully discussed. In this study, low velocity impact tests and high velocity impact tests were performed on glass fiber type E-800 g/m² and type C-600 g/m² specimens with various thicknesses and by varying the impact energy of the drop weight machine and the single gas gun pressure. For high velocity impact testing, it was found that the specimens with the highest thickness and density experienced less damage area. Both glass fiber types showed damage in terms of fiber cracking and fiber pullout after being tested with four different gas gun pressures. Before fiber failure occurs, the laminates will undergo matrix cracking and delamination processes. The type E-800 g/m² specimens exhibited less severe matrix damage than the type C-600 g/m². The experimental results show that the damages on the impacted glass fiber composites are affected by the difference in thickness and the mechanical properties.

For low velocity impact testing, glass fiber type E-800 g/m² had a smaller damage area compared with type C-600 g/m² at all impact energies tested. At the impact of 12J, 14-ply type E-800 g/m² only experienced delamination. Therefore, 14-ply type E-800 g/m² is more impact resistant. The failure modes in this low velocity impact event include delamination and fiber cracking. At the same impact energy level, type C-600 g/m² composite samples experienced more severe matrix damage

than the type E-800 g/m². It can be concluded that glass fiber type E-800 g/m² has greater fiber strength than glass fiber type C-600 g/m². A comparison of glass fiber type E-800 g/m² and type C-600 g/m² established that the type E-800 g/m² is much stronger and resistant to impact damage due to their better fiber strength.

Acknowledgement

This work was supported by the Universiti Putra Malaysia under the research grant UPM/GP-IPS 9482800. Special thanks to the Aerospace Manufacturing Research Centre (AMRC), Universiti Putra Malaysia, and also to the Laboratory of Biocomposite Technology, Institute of Tropical Forestry and Forest Products (INTROP)-HiCOE, Universiti Putra Malaysia.

References

- [1] Seydibeyoglu MO, Mohanty AK, Misra M. Fiber technology for fiber-reinforced composites. Woodhead Publishing; 2017.
- [2] Feng C, Chu Z. Fiber reinforcement. In: Composite materials engineering, vol. 1. Springer; 2018. p. 63–150.
- [3] Bakkal M, Savas M. Development of natural fiber reinforced laminated hybrid composites. *Adv Mater Res* 2012;628:15–20.
- [4] Hajiha H, Sain M. High toughness hybrid biocomposite process optimization. *Compos Sci Technol* 2015;111:44–9.
- [5] Bhudolia SK, Kam KKC, Joshi SC. Mechanical and vibration response of insulated hybrid composites. *J Ind Textil* 2017. 1528083717714481.
- [6] Bulut M, Erklığ A, Yeter E. Hybridization effects on quasi-static penetration resistance in fiber reinforced hybrid composite laminates. *Compos B Eng* 2016;98:9–22.
- [7] Bandaru AK, Vetiyatil L, Ahmad S. The effect of hybridization on the ballistic impact behavior of hybrid composite armors. *Compos B Eng* 2015;76:300–19.
- [8] Randjbaran E, et al. Hybrid composite laminates reinforced with Kevlar/carbon/glass woven fabrics for ballistic impact testing. *ScientificWorldJournal* 2014;2014:413753.
- [9] Petrucci R, et al. Impact and post-impact damage characterisation of hybrid composite laminates based on basalt fibres in combination with flax, hemp and glass fibres manufactured by vacuum infusion. *Compos B Eng* 2015;69:507–15.
- [10] Bo M, Fariborz H, Paridah T. Control and design of volumetric composition in pultruded hybrid fibre composites. *IOP Conf Ser Mater Sci Eng* 2016;139(1):012033.
- [11] Muhammad YH, et al. Mechanical properties of hybrid glass/kenaf fibre-reinforced epoxy composite with matrix modification using liquid epoxidised natural rubber. *J Reinforc Plast Compos* 2015;34(11):896–906.
- [12] Atiqah A, et al. Development of kenaf-glass reinforced unsaturated polyester hybrid composite for structural applications. *Compos B Eng* 2014;56:68–73.
- [13] Wei B, Cao H, Song S. RETRACTED: environmental resistance and mechanical performance of basalt and glass fibers. *Mater Sci Eng A* 2010;527(18–19):4708–15.
- [14] Ashraf W, et al. Investigation of mechanical behavior of woven/knitted hybrid composites. *J Textil Inst* 2017;108(9):1510–7.

- [15] Yan R, et al. Low-velocity impact and static behaviors of high-resilience thermal-bonding inter/intra-ply hybrid composites. *Compos B Eng* 2015;69:58–68.
- [16] Johnson S, Kang LP, Akil HM. Mechanical behavior of jute hybrid bio-composites. *Compos B Eng* 2016;91:83–93.
- [17] Dalbehera S, Acharya SK. Impact of stacking sequence on tribological wear performance of woven jute-glass hybrid epoxy composites. *Tribol Mater Surface Interfac* 2015;9(4): 196–201.
- [18] Murugan R, Ramesh R, Padmanabhan K. Investigation of the mechanical behavior and vibration characteristics of thin walled glass/carbon hybrid composite beams under a fixed-free boundary condition. *Mech Adv Mater Struct* 2016;23(8):909–16.
- [19] Ozben T. Impact behavior of hybrid composite plates dependent on curing and different stacking sequences. *Mater Testing* 2016;58(5):442–7.
- [20] Czél G, Jalalvand M, Wisnom MR. Design and characterisation of advanced pseudo-ductile unidirectional thin-ply carbon/epoxy–glass/epoxy hybrid composites. *Compos Struct* 2016;143:362–70.
- [21] Kalantari M, Dong C, Davies IJ. Multi-objective robust optimisation of unidirectional carbon/glass fibre reinforced hybrid composites under flexural loading. *Compos Struct* 2016;138:264–75.
- [22] Muñoz R, et al. Ballistic performance of hybrid 3D woven composites: experiments and simulations. *Compos Struct* 2015;127:141–51.
- [23] Pandya KS, et al. Ballistic impact behavior of hybrid composites. *Mater Des* 2013;44: 128–35.
- [24] Cerbu C, Botiş M. Numerical modeling of the flax/glass/epoxy hybrid composite materials in bending. *Procedia Eng* 2017;181:308–15.
- [25] Saidane El H, Scida D, Assarar M, Sabhi H, Ayad R. Hybridisation effect on diffusion kinetic and tensile mechanical behaviour of epoxy based flax-glass composites. *Composites Part A* 2016;87.
- [26] Ridzuan MJM, et al. Thermal behaviour and dynamic mechanical analysis of Pennisetum purpureum/glass-reinforced epoxy hybrid composites. *Compos Struct* 2016;152:850–9.
- [27] Rana RS, et al. Characterization of properties of epoxy sisal/glass fiber reinforced hybrid composite. *Mater Today Proc* 2017;4(4):5445–51.
- [28] Hashmi SAR, et al. Development of environment friendly hybrid layered sisal–glass–epoxy composites. *Compos Interfac* 2011;18(8):671–83.
- [29] Angrizani CC, et al. Thermal and mechanical investigation of interlaminar glass/curaua hybrid polymer composites. *J Nat Fibers* 2017;14(2):271–7.
- [30] Ramachandra Reddy G, et al. Tamarind fruit fiber and glass fiber reinforced polyester composites. *Mech Adv Mater Struct* 2015;22(9):770–5.
- [31] Zuhudi NZM, Lin RJ, Jayaraman K. Flammability, thermal and dynamic mechanical properties of bamboo-glass hybrid composites. *J Thermoplast Compos Mater* 2014;29(9): 1210–28.
- [32] Ramesh M, Palanikumar K, Hemachandra Reddy K. Evaluation of mechanical and interfacial properties of sisal/jute/glass hybrid fiber reinforced polymer composites. *Trans Indian Inst Met* 2016;69(10):1851–9.
- [33] Aktaş A, Aktaş M, Turan F. The effect of stacking sequence on the impact and post-impact behavior of woven/knit fabric glass/epoxy hybrid composites. *Compos Struct* 2013;103: 119–35.
- [34] Mitrevski T, Marshall I, Thomson R. The influence of impactor shape on the damage to composite laminates. *Compos Struct* 2006;76(1):116–22.

- [35] Vieille B, Casado VM, Bouvet C. About the impact behavior of woven-ply carbon fiber-reinforced thermoplastic- and thermosetting-composites: a comparative study. *Compos Struct* 2013;101:9–21.
- [36] Bandaru AK, et al. Low velocity impact response of 3D angle-interlock Kevlar/basalt reinforced polypropylene composites. *Mater Des* 2016;105:323–32.
- [37] Sultan MTH, et al. Impact damage characterisation of composite laminates using a statistical approach. *Compos Sci Technol* 2012;72(10):1108–20.
- [38] Sevkát E, et al. Effect of repeated impacts on the response of plain-woven hybrid composites. *Compos B Eng* 2010;41(5):403–13.
- [39] Yashiro S, et al. Characterization of high-velocity impact damage in CFRP laminates: Part I—experiment. *Compos Appl Sci Manuf* 2013;48:93–100.
- [40] García-Castillo SK, et al. Perforation of composite laminate subjected to dynamic loads. In: *Dynamic failure of composite and sandwich structures*. Springer; 2013. p. 291–337.